Comparative Study of Different Constructions of Morphological Leveling Decompositions for Spatial Multi-scale Image Analysis

Nor El Houda Alioua[1(✉)], Samir L' Haddad[1], Akila Kemmouche[1], Alessandra Capolupo[2], and Eufemia Tarantino[2]

[1] Laboratory of Image Processing and Radiation, Department of Telecommunication, Faculty of Electrical Engineering, University of Sciences and Technology Houari Boumediene, Algiers, Algeria
nalioua@usthb.dz

[2] Department of Civil, Environmental, Land, Construction and Chemistry (DICATECh), Politecnico di Bari, Bari, Italy

Abstract. Mathematical morphology is a powerful tool for analyzing the geometrical properties of land cover classes while mitigating spectral confusion in remote sensing data, particularly in hyperspectral images. Among various approaches for modeling spatial information, hierarchical image processing via morphological multi-scale decomposition is a prominent technique for structural image characterization. A key component of this decomposition is morphological leveling, which provides a robust framework for hierarchical image analysis. This study systematically investigates and compares different morphological leveling decomposition strategies using a hyperspectral image acquired in 2002 over the University of Pavia campus in Italy. Two experiments were conducted to assess the impact of different morphological leveling configurations on classification performance. The first experiment evaluated four morphological leveling constructions, each defined by distinct reference and marker parameters combined with three filtering techniques (Gaussian Convolution, Alternate Sequential Filter, and Averaged Alternate Sequential Filter). The second experiment assessed the effectiveness of residual leveling images derived from the results of the first experiment. Outputs from both experiments were integrated with the spectral information and used as input to a two-dimensional convolutional neural network to improve classification accuracy. The analysis of overall accuracy and agreement with ground truth data shows that incorporating morphological leveling significantly enhances classification performance. One configuration achieved nearly 99% accuracy with a very high level of agreement, highlighting the potential of multi-scale spectral–spatial feature extraction. These results offer valuable insights for future applications in remote sensing and environmental monitoring.

Keywords: Mathematical morphology · Morphological leveling · Multi-scale image analysis · Classification · 2D-CNN

© The Author(s), under exclusive license to Springer Nature Switzerland AG 2026
O. Gervasi et al. (Eds.): ICCSA 2025 Workshops, LNCS 15891, pp. 157–174, 2026.
https://doi.org/10.1007/978-3-031-97617-9_11

1 Introduction

Hyperspectral remote sensing employs sensors to capture images of a target area across numerous and contiguous spectral bands simultaneously [1]. Compared to multispectral imaging, HyperSpectral Imaging (HSI) provides richer spectral information, enhancing its ability to accurately identify ground features, particularly for land cover classification [2]. However, relying solely on spectral data presents numerous challenges in image classification. To improve this process, it is recommended to incorporate supplementary data in addition to the hyperspectral bands, like, for instance, spatial features [3]. Mathematical Morphology (MM) is a powerful tool for generating complementary spatial information about image structures.

Several techniques for obtaining spatial information exist, particularly morphological multi-scale decomposition methods, which provide hierarchical image representations by extracting structures at multiple scales. One of the earliest approaches, morphological granulometries and anti-granulometries [4–6], applied sequential openings and closings with Structuring Elements (SEs) of increasing size to analyze object structures. Granulometry utilizes a series of openings, whereas anti-granulometry employs closings to extract features at different scales.

Morphological leveling, introduced by F. Meyer [7–9], is another hierarchical decomposition method based on elementary dilation and erosion. This technique simultaneously decomposes bright and dark structures, ensuring spatial consistency and object contours across scales. Marker/reference images control the transition between scales, enabling hierarchical decomposition. A morphological scale-space representation based on leveling was used to create a fourth-dimensional dataset analyzed via Tensor Principal Components Analysis (TPCA) [10]. Similarly, an additive decomposition by leveling, integrating spatial information into the dimensionality reduction process was proposed [11].

More recently, hierarchical approaches include min-trees, max-trees, inclusion-trees (or tree of shapes), and Binary Partition Trees (BPTs) generate image decompositions based on connected component hierarchies were introduced [12–14]. These structures allow for efficient spatial characterization. On the contrary, the multi-scale image decomposition has also been performed through the Morphological Profiles (MPs) [15–17]. MPs decompose a greyscale image through sequential opening and closing by reconstruction with SEs of increasing size, extracting multi-scale structural features. To extend this approach, two categories of MPs were introduced to model both object length and width [17]: Additive Morphological Decomposition (AMD) and Extended Morphological Profiles (EMPs). The AMD method achieves morphological scale-space decomposition, producing residue images similar to MPs but incorporating an additional term related to image structures, allowing for a more refined representation of spatial features [18]. On the other hand, EMPs were specifically developed for hyperspectral and multispectral images by applying MPs to Principal Components (PCs) extracted via Principal Component Analysis (PCA) [19]. While EMPs enhance feature extraction by modeling shape at different scales, they only

partially characterize objects, as they primarily focus on structural properties while neglecting other spatial attributes such as contrast and texture. To address this, morphological attribute operators were introduced, extracting geometric, textural, and contrast-based primitives [13,20]. Morphological Attribute Profiles (APs) refine MPs by filtering connected components based on morphological attributes rather than fixed SE sizes [21]. APs were further extended for multichannel data, resulting in Extended Attribute Profiles (EAPs), which apply APs to PCs or Feature Components (FCs), enhancing spatial feature extraction [21–23]. Additional hierarchical methods include Multiple Morphological Profiles (MMPs) [22], which integrate EMPs and EAPs from multiple base images, and AMD-based hierarchical representations [23], which model spatial information more effectively. Self-Dual Attribute Profiles (SDAPs) extend APs by simultaneously processing bright and dark structures [24], while Extended Self-Dual Attribute Profiles (ESDAPs) adapt SDAPs for multichannel data through dimensionality reduction techniques [25].

While those morphological approaches provide valuable spatial information, they often rely on predefined SEs and filtering criteria, which may limit their ability to capture complex spatial patterns in HSI. To overcome these limitations and further enhance spatial–spectral feature extraction, deep learning techniques, particularly Convolutional Neural Networks (CNNs), have gained significant interest in recent decades. CNNs have emerged as a promising solution for HIS classification, effectively extracting spectral–spatial features and making them a widely used algorithm for classification tasks [26]. The three common CNN architectures for hyperspectral image classification are one-dimensional (1D-CNN), two-dimensional (2D-CNN), and three-dimensional (3D-CNN). 1D-CNN models employ 1D convolution kernels to process spectral features, treating each pixel vector as 1D data. This approach enables deeper spectral analysis, but distinguishing between different land cover types can be challenging due to spectral mixing effects. 2D-CNN models utilize 2D convolution kernels to extract spatial features from 2D image representations, effectively capturing spatial relationships among neighboring pixels. While this enhances spatial feature extraction, it may overlook crucial spectral correlations. 3D-CNN models integrate both spatial and spectral information using 3D convolution kernels. Despite its effectiveness, the increased model complexity leads to higher computational costs [27].

HSI data typically encompasses various object categories, some of which exhibit distinct spatial features, while others are more easily distinguishable from spectral characteristics. Therefore, integrating spatial information derived from different morphological leveling decompositions with spectral data in CNNs can enhance classification accuracy and efficiency, particularly in multiclass classification tasks.

This paper aims to investigate and compare different constructions of morphological leveling decompositions from the literature to determine which approach yields the most discriminative features for spatial image analysis and achieves the highest classification accuracy using the 2D-CNN model. The

proposed framework showcases its potential for advancing geospatial analysis in urban and environmental applications.

The paper is structured as follows: i) Sect. 2 provides the scientific background of the fundamental's concepts of PCA and morphological leveling; ii) Sect. 3 details the experiment, including a description of the dataset and the classification process; iii) Sect. 4 presents and discusses the results, comparing different approaches and evaluating their effectiveness; iv) finally, Sect. 5 concludes the study, summarizing key findings, limitations and outlines potential directions for future research.

2 Scientific Background

2.1 PCA

PCA is a widely used technique for feature extraction and dimensionality reduction in remote sensing applications, particularly for analyzing HSI [28]. Its objective is to preserve essential information while reducing data's dimensionality. By applying orthogonal transformations, PCA converts highly correlated HSI bands into a set of linearly uncorrelated variables, enabling the extraction of the most informative spectral features [29]. This is achieved by identifying PCs that maximize the variance within the data. In HSI, the data cube is first reshaped into a data matrix D of dimensions $B * A_{\text{Total}}$, where $A_{\text{Total}} = X * Y$ represents the total number of pixels and B is the number of spectral bands. Each spectral vector is denoted as:

$$\mathbf{x}_n = [x_{n1}, x_{n2}, \ldots, x_{nB}]^\top, \quad \text{with} \quad n \in [1, A_{\text{Total}}],$$

where T denotes the transpose operation. Next, the mean image vector is calculated as:

$$M = \frac{1}{A_{\text{Total}}} \sum_{n=1}^{A_{\text{Total}}} x_n \tag{1}$$

The mean-adjusted spectral vectors are: $I_n = x_n - M = [I_{n1}, I_{n2}, \ldots, I_{nB}]^T$, forming a zero-mean image: $I_n = [I_1, I_2, \ldots, I_B]^T$. The covariance matrix is then computed using:

$$C = \frac{1}{A_{\text{Total}}} I * I^T \tag{2}$$

Eigen-decomposition of C yields eigenvectors $(V_1, V_2, \ldots, V_F)$ and corresponding eigenvalues $(E_1, E_2, \ldots, E_F)$, expressed as:

$$C = V * E * V^T \tag{3}$$

The top k components are selected to construct a matrix w of size $B*k$, where k represents the dimensionality of the transformed feature space and satisfies $k \leq B$. Finally, the transformation matrix w is applied to project the original HSI data into the new feature space Y as follows:

$$Y = w^T * I \tag{4}$$

2.2 Morphological Leveling for Multi-scale Imaging Structure Decomposition

Morphological leveling is a powerful tool for multi-scale image decomposition, allowing the extraction of spatial information without distorting or replacing objects in the original data. It produces several levelings, denoted as Λ_i, each obtained by iterating Eq. (5) or Eq. (6) until convergence, where δ and ε represent morphological dilation and erosion, respectively, while"$\wedge$" and "$\vee$" denote the minimum (Infimum) and maximum (Supremum) operations:

$$\Lambda_i : \text{MarkFun}_i = (\text{RefFun} \wedge \delta(\text{MarkFun})) \vee \varepsilon(\text{MarkFun}) \tag{5}$$

$$\Lambda_i : \text{MarkFun}_i = (\text{RefFun} \vee \varepsilon(\text{MarkFun})) \wedge \delta(\text{MarkFun}) \tag{6}$$

The leveling process is completed when the marker function remains unchanged across two successive iterations. The final marker function from the last iteration represents the morphological leveling Λ_i at level i.

The construction of the morphological leveling is guided by the choice of "marker" and "reference" functions. Several approaches have been proposed in literature, among them:

- **Fixed reference function approach:** the reference function is set as the original grey scale across all levels [30,31].
- **Progressive reference function approach:** the reference function at level i is set as the leveling output for the previous level $(i-1)$ [7,9,31].

The marker function, considered as the second parameter of the morphological leveling, is typically derived using a simplification function ψ_i (defined by different filters) applied on the original image or the previous leveling Λ_{i-1}. The degree of simplification increases with each level. Different methods exist for computing marker functions:

- **Alternate Sequential Filters (ASF):** the marker functions are initialized with the original image (MarkFun_0 = original image) and evolve through ASF [9]. At the level i, it is given by:

$$\text{MarkFun}_i = \phi_i\gamma_i(\text{MarkFun}_{i-1}) \tag{7}$$

  where ϕ_i and γ_i are standard closings and openings with SE of size i. The simplification effect is controlled by the SE's size.
- **Averaged Alternate Sequential Filters (AASF):** the marker function is obtained by using the following equation [7]:

$$\text{MarkFun}_i = \frac{\text{ASF1}_{B_i} - \text{ASF2}_{B_i}}{2} \tag{8}$$

  where

$$\text{ASF1}_{B_i} = \phi_i\gamma_i \ldots \phi_2\gamma_2\phi_1\gamma_1\ (\text{f}) \quad \text{and} \quad \text{ASF2}_{B_i} = \gamma_i\phi_i \ldots \gamma_2\phi_2\gamma_1\phi_1(f)$$

– **Gaussian Convolutions:** Gaussian kernel filters with standard deviations σ_i are applied at each level to produce a marker function [9,31]. The multi-scale leveling image decomposition is controlled by the standard deviation "σ" of the Gaussian kernel.

It is particularly useful to explore different morphological leveling constructions and compare the resulting multi-scale decompositions obtained using various marker/reference functions. To obtain multi-scale representation of image by morphological leveling, Λ_i, is based on the following functions (RefFun, MarkFun) applied at each level (lev (RefFun, MarkFun)).

– $\Lambda_i = \text{lev}(f, \psi_i(f))$
– $\Lambda_i = \text{lev}(f, \psi_i(\Lambda_{i-1}))$ with $\Lambda_0 = f$
– $\Lambda_i = \text{lev}(\Lambda_{i-1}, \psi_i(f))$ with $\Lambda_0 = f$
– $\Lambda_i = \text{lev}(\Lambda_{i-1}, \psi_i(\Lambda_{i-1}))$ with $\Lambda_0 = f$

where ψ_i is the filter transformation used to produce marker image at level i. ψ_i can be:

– Gaussian kernel (G_{σ_i}) of standard deviations σ_i;
– ASF_i of size i;
– AASF_i of size i.

For multichannel images, morphological leveling is applied independently to each spectral band. The final multi-scale decomposition consists of the leveling results from all image bands, which are then stacked with spectral responses for spectral-spatial classification. Residual leveling images can be computed to extract additional morphological descriptors which help in feature extraction. The several strategies exist for defining residual images are:

– Difference between the original and the leveling images:

$$R_i = | f - \Lambda_{i-1} | \tag{9}$$

– Differences between successive leveling [7,31]:

$$R_i = | \Lambda_i - \Lambda_{i-1} | \tag{10}$$

– Additive Decomposition by Leveling (ADL) [31]:

$$R_i = (\Lambda_i \times \Lambda_{i-1}) - (\Lambda_{i-1} \times \Lambda_{i-2}) \tag{11}$$

– Difference between leveling and filtered leveling images [9]:

$$R_i = | \Lambda_i - \psi_i(\Lambda_i) | \tag{12}$$

The effectiveness of different morphological leveling constructions and residual images in producing discriminative features for classification is evaluated in this study.

2.3 2D-Convolutional Neural Networks

CNNs have recently been demonstrated to significantly enhance the accuracy of land cover classification for hyperspectral images and efficiently acquire high-level representations of spatial and spectral features [32]. The main task of hyperspectral image processing using CNN architecture is to simultaneously handle spatial and spectral information through adjacent layers. Figure 1 illustrates the structure of the 2D-CNN classification framework with its specific parameters. The 2D-CNN architecture begins with a zero-padding preprocessing step to ensure spatial consistency when extracting patches from the hyperspectral image. This padding function expands the original image by adding a margin of zeros around the edges. Fixed-size patches of $5 * 5$ pixels, centered on each pixel, are then extracted, capturing both spectral and spatial information. The dataset was then split into training (70%), validation (20%), and test (10%) sets, ensuring class balance through stratified sampling. Oversampling was performed by replicating underrepresented samples to address class imbalance. Additionally, data augmentation was applied using random vertical flips, horizontal flips, and rotations (ranging from -180° to +180° in 30° increments) on the training patches to enhance model robustness and variability further.

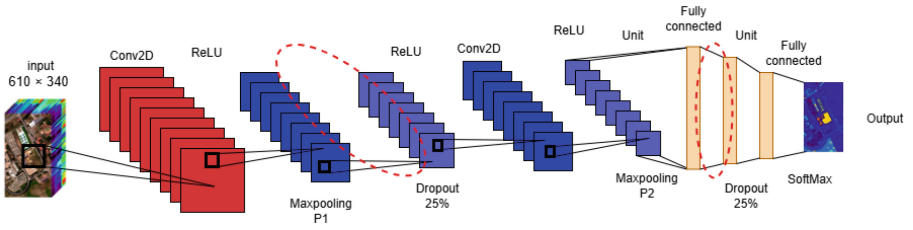

Fig. 1. 2D-CNN architecture.

Feature extraction phase consists of a two-layer convolutional network. The first convolutional layer extracts low level spatial features, while the second captures deeper spatial patterns. Both layers use the Rectified Linear Unit (ReLU) activation function, followed by 25% dropout layer to reduce overfitting and enhance the nonlinearity of the features [33]. The output of the convolutional layers was flattened and passed through a fully connected dense layer with 60 neurons, followed by another 25% dropout layer for regularization. The final classification layer consists of softmax-activated neurons, corresponding to the number of land cover classes. The model is optimized using the Adam optimizer and categorical cross-entropy loss for multi-class classification [34,35].

3 Experiments

This section presents experiments conducted to evaluate and compare different constructions of morphological leveling for enhancing HSI classification. The

first experiment aimed to assess the classification performance of individual leveling constructions, while the second investigated the effectiveness of the possible residual image decompositions obtained from various leveling constructions for improving HSI classification. The methodology adopted in this work to obtain a classification map of the HSI from the Pavia University (PaviaU) dataset is illustrated in Fig. 2.

The PaviaU scene is a widely used dataset for land cover classification and remote sensing image analysis. Its high spatial and spectral resolution makes it particularly valuable for detailed studies of the Earth's surface, including urban land cover classification, vegetation monitoring, object recognition, and research in remote sensing image processing and computer vision.

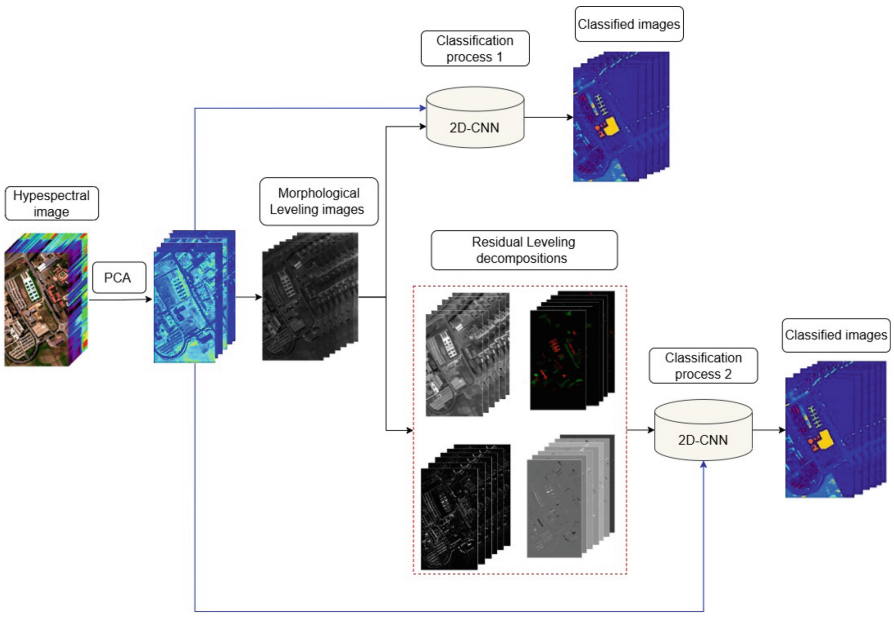

Fig. 2. Flowchart of the proposed spatial–spectral classification methodology.

The first experimental process consisted of three main stages. First, PCA was applied to the original HSI to reduce dimensionality by removing irrelevant and redundant spectral bands (i). During this first step, the number of spectral bands was reduced to 10, retaining the most significant components for subsequent processing. Subsequently, morphological leveling decomposition was performed on each selected PCA band (ii). The decomposition process generated a series of leveled images using different leveling configurations, each defined by distinct reference and marker functions as detailed in Sect 2.2. Specifically, 7 levels were chosen for each PCA image to capture a comprehensive range of spatial features across multiple leveling scales, balancing detail preservation with computational

efficiency. These spatial descriptors were then combined with the PCA spectral bands and used as input features for the 2D-CNN classifier, with the classification rates serving as the evaluation metrics (iii). This experiment tested 12 alternative configurations, each representing a unique reference/marker function combination, yielding 12 classification settings.

In the second experiment, residual leveling images were computed to extract additional morphological descriptors using the strategies mentioned in Sect 2.2. These residuals were derived from the series of leveling images generated in the first experiment, resulting in four series of residual decompositions, each capturing unique spatial characteristics. For each residual decomposition strategy, 12 classification evaluations were performed, resulting in a total of 48 configurations for this experiment. These residual images were then added to the PCA spectral bands and used as input features for the 2D-CNN classifier to investigate their effectiveness in enhancing classification performance.

To assess the effectiveness of the 2D-CNN model, training was conducted over 20 epochs, using the validation set for performance monitoring. The suggested architecture's performance was quantitatively evaluated using the Overall Accuracy (OA) and Kappa coefficient (K) metrics. OA is the percentage of correctly classified pixels divided by the total number of classified pixels [36]. K reflects the consistency between the classified image and the ground truth image, ranging from -1 to 1, with values typically greater than 0 [37].

3.1 Dataset Description

The experiments were conducted on the PaviaU scene, captured in Pavia, Italy, in 2002 by the Reflective Optics System Imaging Spectrometer (ROSIS) sensor [38]. This image consists of 610×340 pixels, with a spatial resolution of 1.3 m/pixel. Initially, the number of data channels was 115, with a spectral range from 0.43 to 0.86 µm. After removing low Signal-to-Noise Ratio (SNR) bands, 103 bands were retained for the experiments.

Table 1. Land use types listed in the ground truth map, as well as the amount of samples supplied for each of them.

#	Class	Samples
1	Asphalt	6631
2	Meadows	18649
3	Gravel	2099
4	Trees	3064
5	Metal sheets	1345
6	Bare Soil	5029
7	Bitumen	1330
8	Self-Blocking Bricks	3682
9	Shadows	947

The dataset is accompanied with a ground truth map that includes nine classes of interest, as shown in Table 1, as well as the number of training and test samples for each class (see Fig. 3). No further preprocessing was required, owing to the dataset's high-quality acquisition and comprehensive ground truth annotations.

This dataset is widely used as a standard dataset for the classification of urban structures in hyperspectral images.

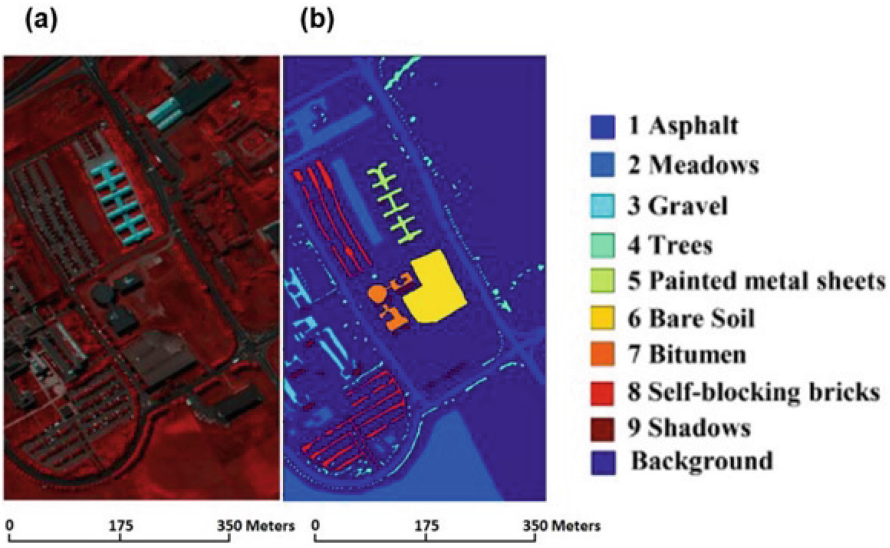

Fig. 3. PaviaU dataset: (a) false-color image, (b) ground-truth image.

4 Results and Discussion

To evaluate the performance of different leveling methods, two main tests were conducted in this study. The first aimed to assess the classification performance of various individual leveling families, using different reference/marker functions to determine how effectively each method preserves and enhances relevant spatial structures, thereby contributing to classification accuracy. Table 2 presents the classification performance of different morphological leveling methods based on OA and K metrics.

Among the tested methods, the highest classification performance was observed when the original spectral bands were used as the marker function $(f, \psi_i(f))$ in conjunction with G_{σ_i} filter, achieving an OA of 89.52% and K of 0.88. This combination preserved both spatial and spectral information, thus

improving classification accuracy. Conversely, when the same configuration was applied using ASF_i and $AASF_i$ filters, lower classification performance was observed, indicating that these filters may not be effectively preserve relevant structural features in this context.

Table 2. Classification rates using Morphological Leveling images Λ_i

(RefFun, MarkFun)	ψ_i	OA (%)	K
$(f, \psi_i(f))$	ASF_i	84.89	0.83
	$AASF_i$	78.72	0.71
	$\mathbf{G_{\sigma_i}}$	**89.52**	**0.88**
$(f, \psi_i(\Lambda_{i-1}))$ with $\Lambda_0 = f$	ASF_i	**87.31**	**0.87**
	$AASF_i$	76.01	0.76
	G_{σ_i}	80.94	0.79
$(\Lambda_{i-1}, \psi_i(f))$ with $\Lambda_0 = f$	ASF_i	85.19	0.80
	$\mathbf{AASF_i}$	**88.19**	**0.85**
	G_{σ_i}	80.31	0.83
$(\Lambda_{i-1}, \psi_i(\Lambda_{i-1}))$ with $\Lambda_0 = f$	ASF_i	82.23	0.80
	$\mathbf{AASF_i}$	**86.07**	**0.84**
	G_{σ_i}	79.94	0.72

However, when the recursive marker function $\psi_i(\Lambda_{i-1})$ was used with $\Lambda_0 = f$, the ASF_i filter produced the best results, achieving an OA of 87.31% and K of 0.87. In this configuration, the $AASF_i$ and Gaussian-based leveling performed poorly, with significantly lower OA values of 76.01% and 80.94%, respectively.

Moreover, when a recursive reference function to the initial image was applied, the use of $AASF_i$ filter on the recursive mask function showed the best performance, achieving an OA of 88.19% and a K of 0.85. This suggests that the $AASF_i$ preserved meaningful spatial information while reducing noise. In the final leveling approach, where both the reference and marker functions were recursively applied, the $AASF_i$ filter performed well again, with an OA of 86.07% and a K of 0.84, while Gaussian-based leveling remained stable but did not reach the highest performance. These findings suggest that the ASF_i filter performs better when used with the recursive marker function on the original image, whereas the $AASF_i$ benefits most from a recursive reference function, and Gaussian-based leveling excels when applied directly to the original images. This highlights the importance of selecting the appropriate leveling method based on the desired balance between spectral and spatial feature preservation. Overall, the results indicate that Gaussian-based leveling performs optimally when applied directly to spectral images.

In addition to the quantitative evaluation, a visual assessment of classification maps was performed to compare the leveling approaches. Figure 4 showcases the classification maps obtained by the best performing leveling configurations. As shown, $(f, \psi_i(f))$ with G_{σ_i} filter contained more homogeneous spatial structures and consistently outperformed other approaches. The classification maps produced by this configuration exhibited more clarity with some misclassified pixels, further demonstrating its ability to capture the complex spatial and spectral information present in the PaviaU dataset. The visually compelling results further reinforce the potential of the leveling methods in HSI classification tasks. Although integrating 2D-CNN with morphological leveling enhances spatial feature extraction, the results showed that it does not achieve optimal accuracy. While certain configurations improve classification outcomes, overall performance remains limited, suggesting the need for further refinements in the leveling process or the exploration of alternative feature extraction strategies to better exploit spatial and spectral information.

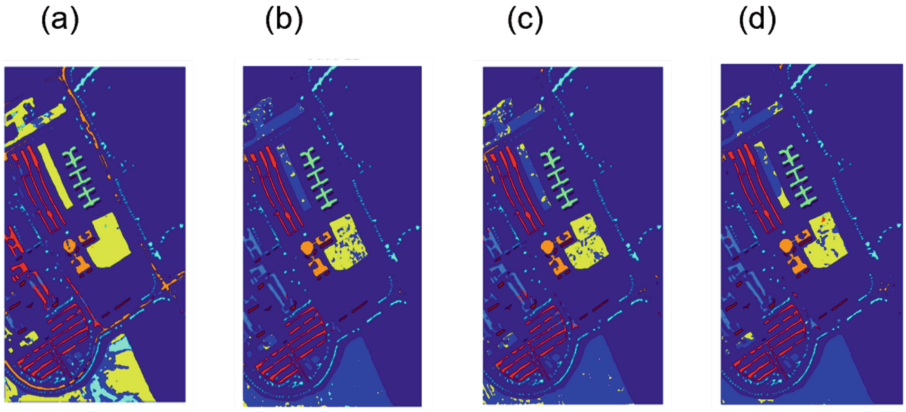

Fig. 4. G_{σ_i}.

The second test further analyzed the impact of morphological leveling on classification by investigating the performance of residual images generated by different leveling methods. These residual images captured the differences between consecutive levels of decomposition, highlighting fine-scale spatial structures and variations that provide additional discriminative features for classification. By computing multiple morphological leveling constructions with different reference and marker functions, the study assessed the impact of various spatial descriptors on classification performance. Finally, a comparative analysis was conducted to

evaluate the efficiency of each approach, providing insights into the effectiveness of morphological leveling in enhancing classification accuracy and identifying the most suitable technique for HSI analysis.

Table 3 presents the classification accuracy rates obtained from different morphological leveling decompositions for HSI classification. Various decomposition strategies were evaluated based on their impact on 2D-CNN performance. The methods compared included level residual images $|\Lambda_i - \Lambda_{i-1}|$, ADL $(\Lambda_i \times \Lambda_{i-1}) - (\Lambda_{i-1} \times \Lambda_{i-2})$, residual images $|\text{MarkFun} - \Lambda_i|$, and difference images $|f - \Lambda_i|$. Each decomposition method was assessed across the different filter strategies.

Table 3. Classification rates using different residual image decompositions

Morphological leveling decompositions	ψ_i	$\|\Lambda_i - \Lambda_{i-1}\|$		$(\Lambda_i \times \Lambda_{i-1}) - (\Lambda_{i-1} \times \Lambda_{i-2})$		$\|\text{MarkFun} - \Lambda_i\|$		$\|f - \Lambda_i\|$	
		OA (%)	K	OA (%)	K	OA (%)	K	OA (%)	K
$(f, \psi_i(f))$	ASF_i	**97.24**	**0.96**	73.98	0.67	**82.02**	**0.79**	81.67	0.67
	$AASF_i$	95.85	0.93	88.71	0.85	74.03	0.66	74.03	0.71
	G_{σ_i}	94.37	0.92	**94.37**	**0.92**	**87.05**	0.83	**87.05**	**0.88**
$(f, \psi_i(\Lambda_{i-1}))$ with $\Lambda_0 = f$	ASF_i	92.57	0.90	91.02	0.88	79.50	0.73	86.55	0.85
	$AASF_i$	89.25	0.86	91.77	0.89	79.78	0.72	88.05	0.84
	G_{σ_i}	**95.59**	**0.95**	**92.19**	**0.90**	**89.46**	**0.86**	**95.80**	**0.92**
$(\Lambda_{i-1}, \psi_i(f))$ with $\Lambda_0 = f$	ASF_i	90.51	0.88	**93.90**	**0.91**	76.25	0.68	76.04	0.68
	$AASF_i$	92.17	0.89	92.52	0.90	63.32	0.59	72.77	0.64
	G_{σ_i}	**95.21**	**0.93**	96.00	0.94	**77.33**	**0.70**	**89.65**	**0.83**
$(\Lambda_{i-1}, \psi_i(\Lambda_{i-1}))$ with $\Lambda_0 = f$	ASF_i	90.37	0.78	93.76	0.91	91.68	0.89	87.93	0.82
	$AASF_i$	**91.40**	**0.89**	**92.36**	**0.90**	79.62	0.74	79.05	0.88
	G_{σ_i}	90.81	0.89	94.92	**0.92**	**94.67**	**0.92**	**98.90**	**0.98**

The results indicate that the highest classification performance was achieved using the difference images $|f - \Lambda_i|$ decomposition, particularly when combined with the G_{σ_i} filter, resulting in an OA of 98.90% and a K of 0.98. This suggests that incorporating spectral and spatial information through morphological leveling significantly enhances classification accuracy. The results also demonstrate the effectiveness of ADL in capturing multi-scale texture components through successive leveling operations. This observation aligns with previous studies [10]. By utilizing three recursive levels of morphological leveling (Λ_i, Λ_{i-1}, and Λ_{i-2}), ADL effectively extracts discriminative spatial structures that improve classification accuracy.

Performance varied depending on the choice of reference and marker functions. The $(\Lambda_{i-1}, \psi_i(f))$ *with* $\Lambda_0 = f$ configuration consistently achieved the highest OA and K values across all configurations, reaching 96.00% OA and 0.94 K when using the G_{σ_i} filter. This demonstrates its effectiveness in preserving meaningful texture information across multiple scales. The results

emphasize the importance of selecting an appropriate combination of reference/marker functions, with the consistent performance using G_{σ_i} filter across all configurations highlighting its robustness in extracting meaningful spatial features for classification.

Figure 5 illustrates the impact of different morphological leveling decompositions. The visual comparison indicates that hierarchical decomposition methods effectively enhance spatial feature extraction, leading to improved classification accuracy. The classification maps demonstrate a reduction in misclassified pixels, particularly in complex urban areas, where the preservation of spatial structures is evident. This suggests that morphological leveling contributes to improved class separability. Notably, the best-performing decomposition approach produces clearer and more homogeneous class regions, minimizing misclassifications. However, some residual noise remains in certain areas, particularly due to the classifier limitations, indicating that further feature extraction refinements could enhance classification performance. While the tested methods demonstrate significant improvements in HSI classification, they also have limitations that offer avenues for future research. Despite the integration of 2D-CNN layers to balance computational efficiency, the overall computational cost remains relatively high, with training and testing times reaching 1263.04 s and 84.25 s, respectively. This complexity poses challenges for scaling the model to applications involving large datasets. However, previous research has investigated the computational efficiency of different CNN architectures, 1D-CNN, 2D-CNN, 3D-CNN, and hybrid CNNs in hyperspectral image classification [27,39,40]. These studies indicate that 1D-CNNs offer the highest efficiency, 2D-CNNs balance accuracy and computational cost, and 3D-CNNs require most resources due to their use of 3D kernels, which significantly increase computational complexity and extend training and inference times. In future work, the impact of alternative deep learning architectures, such as 1D-CNN, 3D-CNN, and hybrid models, will be explored to provide a more comprehensive evaluation of their relative performance.

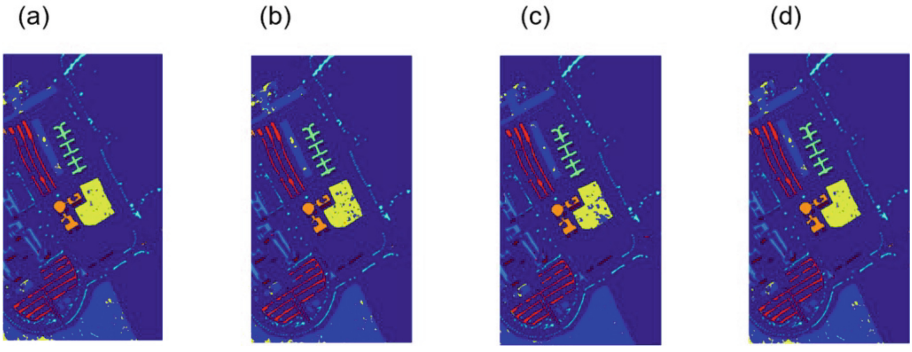

Fig. 5. (a) level residual images $|\Lambda_i - \Lambda_{i-1}|$, (b) ADL $(\Lambda_i \times \Lambda_{i-1}) - (\Lambda_{i-1} \times \Lambda_{i-2})$, (c) residual images $|\text{MarkFun} - \Lambda_i|$, and (d) difference images $|f - \Lambda_i|$.

Although the model generalizes well across the evaluated dataset, further validation on additional, more diverse datasets is necessary to confirm its adaptability to varying environments and spectral conditions. Expanding its application to domains, such as agriculture, environmental monitoring, and urban mapping, could further demonstrate its robustness and scalability in real-world scenarios. Finally, exploring optimization techniques could significantly enhance the model's scalability and suitability.

5 Conclusion

HSI classification is a vital task in remote sensing, with significant implications for agriculture, environmental, monitoring, and urban planning. Despite advancements in deep learning-based classification methods, achieving high accuracy remains challenging due to the complexity of hyperspectral data, its high dimensionality, and the need for effective spatial-spectral feature extraction. Traditional approaches often prioritize spectral information while overlooking valuable spatial structures that could enhance classification performance. Based on this perspective, this study compares and investigates the impact of morphological leveling decompositions on HSI classification by integrating multi-scale spatial features into a 2D-CNN framework. By systematically evaluating different leveling configurations using various reference and marker functions, the study demonstrates that morphological leveling effectively captures spatial structures while preserving object contours. The results highlight that although certain configurations improve classification accuracy, no single leveling approach is optimal overall. Instead, the effectiveness of each method depends on its ability to balance noise reduction and feature enhancement, underscoring the relevance of adopting optimization strategies for reference and marker functions to adaptively tune these parameters for different data characteristics and classification tasks.

Extensive experiments on the PaviaU dataset showed that integrating descriptors from morphological leveling enhances classification performance by highlighting the effectiveness of different constructions. However, the selection of the optimal configuration (reference/marker function combinations, filters, decomposition levels) requires manual tuning and experimentation, which could be time-consuming. Thus, an Auto-ML framework opens new perspectives to systematically automate the process of selecting these parameters.

Although 2D-CNN with leveling improves spatial feature representation, it does not achieve optimal accuracy, suggesting the need for further refinements in feature extraction strategies and deep learning architectures. Furthermore, while the morphological leveling methods enhances spatial feature, its computational cost remains a limiting factor, particularly for large-scale datasets. Future research could explore more efficient morphological decomposition strategies that maintain classification accuracy while reducing computational complexity. Another promising direction could involve the development of hybrid deep learning model to address data scarcity challenges.

Acknowledgments. This study was carried out within the Space It Up project funded by the Italian Space Agency, ASI, and the Ministry of University and Research, MUR, under contract n. 2024-5-E.0 - CUP n. I53D24000060005.

References

1. Liao, W., et al.: Classification of hyperspectral data over urban areas using directional morphological profiles and semi-supervised feature extraction. IEEE J. Sel. Top. Appl. Earth Obs. Remote Sens. **5**(4), 1177–1190 (2012)
2. Ferrato, L.J., Forsythe, K.W.: Comparing hyperspectral and multispectral imagery for land classification of the Lower Don River. Toronto. J. Geogr. Geol. **5**(1), 92–107 (2013)
3. Huang, X., et al.: Multiple morphological profiles from multicomponent-base images for hyperspectral image classification. IEEE J. Sel. Top. Appl. Earth Obs. Remote Sens. **7**(12), 4653–4669 (2014)
4. Fauvel, M., Tarabalka, Y., Benediktsson, J.A., Chanussot, J., Tilton, J.C.: Advances in spectral-spatial classification of hyperspectral images. Proc. IEEE **101**(3), 652–675 (2013)
5. Maragos, P.: Pattern spectrum and multiscale shape representation. IEEE Trans. Pattern Anal. Mach. Intell. **11**, 701–716 (1989)
6. Vincent, L.: Granulometries and opening trees. Fundam. Inform. **41**(1–2), 57–90 (2000)
7. Meyer, F.: The levelings. In: Heijmans, H., Roerdink, J. (eds.) Mathematical Morphology and Its Applications to Image and Signal Processing, pp. 199–206. Kluwer (1998)
8. Meyer, F., Maragos, P.: Nonlinear scale-space representation with morphological levelings. J. Vis. Commun. Image Represent. **11**(2), 245–265 (2000)
9. Meyer, F.: Levelings, image simplification filters for segmentation. J. Math. Imaging Vis. **20**, 59–72 (2004)
10. Velasco-Forero, S., Angulo, J.: Morphological scale-space for hyperspectral images and dimensionality exploration using tensor modeling. In: IEEE Workshop on Hyperspectral Image and Signal Processing: Emerging Remote Sensing (WHISPERS), pp. 1–4. IEEE (2009)
11. Velasco-Forero, S., Angulo, J.: Classification of hyperspectral images by tensor modeling and additive morphological decomposition. Pattern Recogn. **46**(2), 566–577 (2013)
12. Salembier, P., Oliveras, A., Garrido, L.: Antiextensive connected operators for image and sequence processing. IEEE Trans. Image Process. **7**(4), 555–570 (1998)
13. Salembier, P., Garrido, L.: Binary partition tree as an efficient representation for image processing, segmentation, and information retrieval. IEEE Trans. Image Process. **9**(4), 561–576 (2000)
14. Monasse, P., Guichard, F.: Fast computation of a contrast-invariant image representation. IEEE Trans. Image Process. **9**(5), 860–872 (2000)
15. Pesaresi, M., Benediktsson, J.: A new approach for the morphological segmentation of high-resolution satellite imagery. IEEE Trans. Geosci. Remote Sens. **39**(2), 309–320 (2001)
16. Plaza, A., et al.: Advanced processing of hyperspectral images. Remote Sens. Environ. **113**(1), S110–S122 (2009)

17. Dalla Mura, M., Benediktsson, J.A., Chanussot, J., Bruzzone, L.: The evolution of the morphological profile: from panchromatic to hyperspectral images. In: Optical Remote Sensing - Advances in Signal Processing and Exploitation Techniques. Springer, Cham (2011)
18. Bellens, R., et al.: Improved classification of VHR images of urban areas using directional morphological profiles. IEEE Trans. Geosci. Remote Sens. **46**(10), 2803–2813 (2008)
19. Benediktsson, J.A., Palmason, J.A., Sveinsson, J.R.: Classification of hyperspectral data from urban areas based on extended morphological profiles. IEEE Trans. Geosci. Remote Sens. **43**(3), 480–491 (2005)
20. Dalla Mura, M., et al.: Morphological attribute filters for the analysis of very high-resolution remote sensing images. In: IEEE International Geoscience and Remote Sensing Symposium (IGARSS), vol. 3, pp. III–97–III–100. IEEE (2009)
21. Breen, E.J., Jones, R.: Attribute openings, thinnings, and granulometries. Comput. Vis. Image Underst. **64**(3), 377–389 (1996)
22. Dalla Mura, M., et al.: Morphological attribute profiles for the analysis of very high-resolution images. IEEE Trans. Geosci. Remote Sens. **48**(10), 3747–3762 (2010)
23. Dalla Mura, M., et al.: Extended profiles with morphological attribute filters for the analysis of hyperspectral data. Int. J. Remote Sens. **31**(22), 5975–5991 (2010)
24. Dalla Mura, M., et al.: Self-dual attribute profiles for the analysis of remote sensing images. In: Mathematical Morphology and Its Applications to Image and Signal Processing, pp. 320–330. Springer, Cham (2011)
25. Cavallaro, G., et al.: Extended self-dual attribute profiles for the classification of hyperspectral images. IEEE Geosci. Remote Sens. Lett. (2015)
26. Mei, X., et al.: Spectral-spatial attention networks for hyperspectral image classification. Remote Sen. **11**(8), 963 (2019)
27. Liu, J., et al.: Integrated 1D, 2D, and 3D CNNs enable robust and efficient land cover classification from hyperspectral imagery. Remote Sens. **15**(19), 4797 (2023)
28. Rodarmel, C., Shan, J.: Principal component analysis for hyperspectral image classification. ACM Surv. Land Inf. Syst. **62**(2), 115–122 (2002)
29. Uddin, M.P., Mamun, M.A., Afjal, M.I., Hossain, M.A.: Information-theoretic feature selection with segmentation-based folded principal component analysis (PCA) for hyperspectral image classification. Int. J. Remote Sens. **42**(1), 286–321 (2021)
30. Gomila, C., Meyer, F.: Levelings in vector spaces. In: Proceedings of IEEE Conference on Image Processing, Kobe, Japan, 24–28 October 1999
31. Angulo, J., Velasco-Forero, S.: Structurally adaptive mathematical morphology on nonlinear scale-space representations. In: ICIP, vol. 17, 121–124 (2010)
32. Gao, Q., Lim, S., Jia, X.: Hyperspectral image classification using convolutional neural networks and multiple feature learning. Remote Sen. **10**(2), 299 (2018)
33. Srivastava, N., Hinton, G., Krizhevsky, A., Sutskever, I., Salakhutdinov, R.: Dropout: a simple way to prevent neural networks from overfitting. J. Mach. Learn. Res. **15**(1), 1929–1958 (2014)
34. Kingma, D.P., Ba, J.: Adam: a method for stochastic optimization. arXiv preprint arXiv:1412.6980 (2014)
35. Hui, L., Belkin, M.: Evaluation of neural architectures trained with square loss vs cross-entropy in classification tasks. arXiv preprint arXiv:2006.07322 (2020)
36. Yuan, D.: A simulation comparison of three marginal area estimators for image classification. Photogramm. Eng. Remote Sens. **53**(4) (1997)
37. Rwanga, S.S., Ndambuki, J.M.: Accuracy assessment of land use/land cover classification using remote sensing and GIS. Int. J. Geosci. **8**(4), 611 (2017)

38. Grupo de Inteligencia Computacional (GIC): Hyperspectral Remote Sensing Scenes. https://www.ehu.eus/ccwintco/index.php/HyperspectralRemoteSensing Scenes\PaviaCentreandUniversity. Accessed 26 Oct 2023
39. Roy, S.K., Krishna, G., Dubey, S.R., Chaudhuri, B.B.: HybridSN: exploring 3-D–2-D CNN feature hierarchy for hyperspectral image classification. IEEE Geosci. Remote Sens. Lett. **17**, 277–281 (2020)
40. Paoletti, M.E., Haut, J.M., Plaza, J., Plaza, A.: A new deep convolutional neural network for fast hyperspectral image classification. ISPRS J. Photogramm. Remote. Sens. **145**, 120–147 (2018)